

ELASTIC AND INELASTIC SCATTERING
OF ^{15}N IONS BY ^{12}C AT 81 MeV AND THE EFFECT
OF TRANSFER CHANNELS

A.T. RUDCHIK^a, A.A. RUDCHIK^a, O.E. KUTSYK^a, K.W. KEMPER^b
S. KLICZEWSKI^c, K. RUSEK^d, E. PIASECKI^d, A. TRZCIŃSKA^d
E.I. KOSHCHY^e, VAL.M. PIRNAK^a, O.A. PONKRATENKO^a, I. STROJEK^f
V.A. PLUJKO^g, A. STOLARZ^d, S.B. SAKUTA^h, R. SIUDAK^c
O.V. HERASHCHENKO^a, A.P. ILYIN^a, YU.M. STEPANENKO^a
YU.O. SHYRMA^a, V.V. ULESHCHENKO^a

^aInstitute for Nuclear Research, Ukrainian Academy of Sciences
Prospect Nauki 47, 03680 Kyiv, Ukraine

^bPhysics Department, Florida State University, Tallahassee, FL 32306-4350, USA

^cH. Niewodniczański Institute of Nuclear Physics Polish Academy of Sciences
Radzikowskiego 152, 31-342 Kraków, Poland

^dHeavy Ion Laboratory, University of Warsaw
L. Pasteura 5A, 02-093 Warszawa, Poland

^eCyclotron Institute Texas A&M University, College Station, TX 77843, USA

^fNational Center for Nuclear Research, A. Sołtana 7, 05-400 Otwock, Poland

^gTaras Shevchenko National University, Volodymyrska 64, 01033 Kyiv, Ukraine

^hRussian Research Center “Kurchatov Institute”
Kurchatov Sq. 1, 123182 Moscow, Russia

(Received November 9, 2018; accepted March 11, 2019)

Angular distributions of the $^{15}\text{N}+^{12}\text{C}$ elastic and inelastic scattering were measured at $E_{\text{lab}}(^{15}\text{N}) = 81$ MeV to study the nuclear–nuclear interactions and possible transfer contributions to the scattering. The data were analyzed with the coupled-reaction-channels (CRC) method using the $^{15}\text{N}+^{12}\text{C}$ optical potential of Woods–Saxon shape. The elastic and inelastic scattering as well as the most obvious one- and two-step transfer reactions were included in the channel-coupling scheme. The $^{15}\text{N}+^{12}\text{C}$ optical potential and deformation parameters of ^{15}N were deduced. The transfer reaction contributions to the $^{15}\text{N}+^{12}\text{C}$ elastic and inelastic scattering channels were estimated. The $^{15}\text{N}+^{12}\text{C}$ elastic scattering at 81 MeV was compared with the $^{14}\text{N}+^{12}\text{C}$ elastic scattering of ^{14}N beam energy 78 MeV.

1. Introduction

Studies of the elastic and inelastic scattering between $1p$ -shell nuclei have shown a wide variety of reaction contributions to their interaction that is most easily probed by obtaining data at large angles through carrying out the experiments in inverse kinematics. By scattering the heavier beam particle from the lighter mass target and then detecting both particles at forward angles, it has been possible to gather data simultaneously for the forward and backward hemispheres. The results of these studies show that the forward angle data are well-described by potential scattering and the differences in the potentials that describe them reflect isotopic effects between the interacting pairs. It is in the backward hemisphere scattering data that the internal structure of the interacting pairs is probed, with cross sections there varying by factors of ten. It has been possible to study the processes contributing to the scattering through the use of coupled-reactions-channels (CRC) calculations that include various contributions such as from ground state reorientation of nuclei with large ground state quadrupole moments like ${}^9\text{Be}$, or nucleon transfers between the interacting pairs. The study of the inelastic scattering has allowed the extraction of deformation parameters for a large number of excited states in these $1p$ -shell nuclei and it has been possible to determine their impact on the forward angle elastic scattering.

In the present work, the elastic and inelastic scattering of ${}^{15}\text{N}$ ions by ${}^{12}\text{C}$ were measured at the energy $E_{\text{lab}}({}^{15}\text{N}) = 81$ MeV together with the ${}^{12}\text{C}({}^{15}\text{N}, X)$ transfer reactions with stable and unstable nuclei in the exit channels over the full angular range through the use of inverse kinematics. This beam-target combination allows the contribution of potential scattering to the large angle data to be studied. A previous work [1] that focused on measuring resonances in the compound system ${}^{27}\text{Al}$ through the ${}^{12}\text{C}({}^{15}\text{N}, \alpha)$ reaction, also included ${}^{15}\text{N}+{}^{12}\text{C}$ elastic scattering data measured at energies $E_{\text{lab}}({}^{15}\text{N}) = 22.4$ to 31.4 MeV for $\theta_{\text{cm}} > 140^\circ$ to search for correlations between any structures seen in the alpha elastic channels. These large angle elastic data were also analyzed in the present work to further quantify the energy dependence of the potential parameters found from the present higher energy analysis. In addition, the new data were compared with ${}^{14}\text{N}+{}^{12}\text{C}$ scattering data at the energy $E_{\text{lab}}({}^{14}\text{N}) = 78$ MeV [2] to study isotopic effects in the ${}^{14,15}\text{N}+{}^{12}\text{C}$ interactions and scatterings.

To explore the possible contributions of the transfer channels to the ${}^{15}\text{N}+{}^{12}\text{C}$ elastic and inelastic scattering data, CRC calculations were carried out. The spectroscopic amplitudes of nucleons and clusters needed for the CRC calculations were calculated within translational invariant shell model.

The paper is organized as follows. Section 2 contains a brief summary of the experimental procedure, Section 3 gives the results of CRC calculations, and the last section provides a summary of this work.

2. Experimental procedure

Angular distributions of the $^{15}\text{N}+^{12}\text{C}$ elastic and inelastic scattering were measured simultaneously with the $^{12}\text{C}(^{15}\text{N}, X)$ transfer reactions with an 81 MeV beam of ^{15}N from the cyclotron U-200P of the Heavy Ion Laboratory (HIL) of the University of Warsaw. The beam energy spread on the target did not exceed 0.5%. A self-supporting $\sim 500 \mu\text{g}/\text{cm}^2$ foil of natural carbon was used as the target.

The experimental set-up ICARE [3] was used to perform the measurements. The ICARE system consists of the 1 m diameter reaction chamber with up to 48 ΔE - E gas and semiconductor telescopes, supplied with the electronics and data acquisitions systems. The detectors can be mounted in any configuration preferred by users, using internal mounts. The self-supporting target holder allows using up to 6 different targets. Angle and target changes can be operated remotely without the necessity of opening the reaction chamber.

The reaction products were detected by four silicon ΔE - E telescopes with the $40 \mu\text{m}$ silicon ΔE -detectors and 0.3 mm silicon E -detectors.

A typical $\Delta E(E)$ spectrum of the $^{12}\text{C}(^{15}\text{N}, X)$ reaction products is shown in Fig. 1. As one can see, the reaction products with $Z = 3-8$ were well-resolved by charge as well as mass.

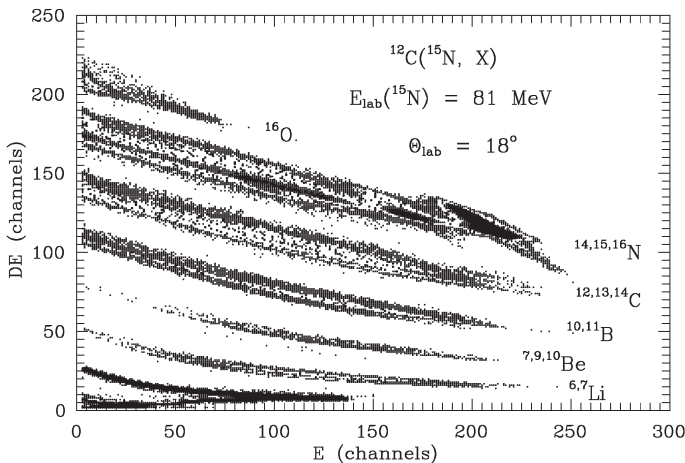


Fig. 1. Typical $\Delta E(E)$ spectrum of the $^{12}\text{C}(^{15}\text{N}, X)$ reaction products.

The areas under the peaks of the residual ^{15}N and ^{12}C spectra were used for obtaining the elastic and inelastic scattering angular distributions. The scattering angle θ_{cm} was related to the angles of the registered ions in the following way: $\theta_{\text{cm}} = \theta_{\text{cm}}(^{15}\text{N})$ and $\theta_{\text{cm}} = 180^\circ - \theta_{\text{cm}}(^{12}\text{C})$. In this way, the angular distributions for the $^{12}\text{C}(^{15}\text{N}, ^{15}\text{N})^{12}\text{C}$ scattering were determined over the whole angular range.

The area errors of the peaks were estimated to be about 20%, if the peaks were well-resolved and 30–40% for poorly resolved peaks. These errors were greater than the statistical errors.

The angular distribution of the $^{15}\text{N}+^{12}\text{C}$ elastic scattering were normalized to the OM cross section at small angles where it is relatively independent of the nuclear potential parameters. The χ^2 -criterion was used to obtain the normalization factor. The normalization error was smaller than 20%. The same factor was used to normalize the angular distribution for the elastic and inelastic scattering data at forward and backward angles.

3. Data analysis

The data of the $^{15}\text{N}+^{12}\text{C}$ elastic and inelastic scatterings were analyzed with the CRC method using the optical model potentials in the entrance and exit channels of Woods–Saxon (WS) form

$$U_{\text{WS}}(r) = -V_0 \left[1 + \exp \left(\frac{r - R_V}{a_V} \right) \right]^{-1} - iW_S \left[1 + \exp \left(\frac{r - R_W}{a_W} \right) \right]^{-1}. \quad (1)$$

Here,

$$R_i = r_i \left(A_P^{1/3} + A_T^{1/3} \right) \quad (i = V, W, C),$$

where A_P, A_T and Z_P, Z_T are the mass and charge numbers of ^{15}N and ^{12}C , respectively. The Coulomb potentials of a uniform charged sphere was used

$$V_C(r) = \begin{cases} Z_P Z_T e^2 (3 - r^2) / 2R_C, & r \leq R_C, \\ Z_P Z_T e^2 / r, & r > R_C, \end{cases} \quad (2)$$

with the parameter $r_C = 1.25$ fm.

In the CRC analysis, the $^{15}\text{N}+^{12}\text{C}$ elastic and inelastic scattering for the transitions to the ground and excited states of ^{12}C and ^{15}N as well as most important transfer reactions were included in the channels coupling scheme.

The transitions to the excited states of ^{12}C and ^{15}N are shown in Fig. 2. Concerning the reaction channels, one-step exchange of triton as well as various two-step processes were included in the analysis (see Fig. 3).

It was assumed that the rotations and vibrations of the deformed ^{12}C and ^{15}N nuclei dominate their low-energy nuclear excitations. The transitions to these states were calculated using the standard form factors

$$V_\lambda(r) = -\frac{\delta_\lambda}{\sqrt{4\pi}} \frac{dU(r)}{dr}, \quad (3)$$

where δ_λ is the length of λ -multipole deformation. The values of the deformation parameters δ_λ and $\beta_\lambda = \delta_\lambda / R$ ($R = 1.25 A^{1/3}$) of ^{12}C and ^{15}N in the ground states taken from Refs. [4, 5] and deduced in this work are listed in Table I.

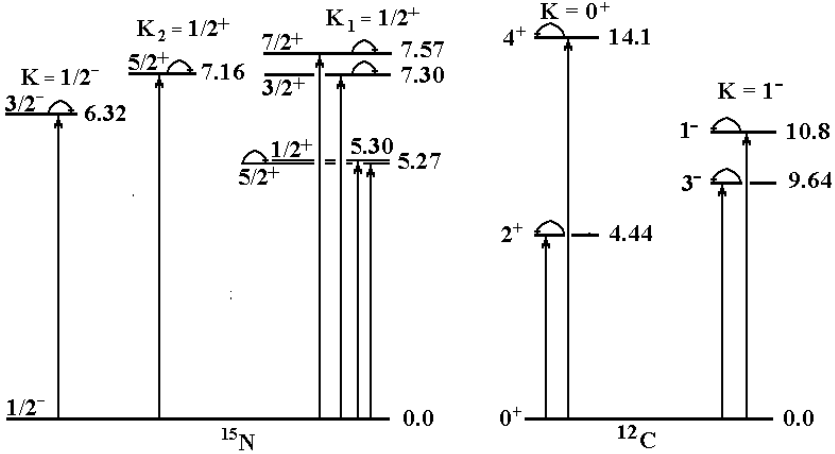


Fig. 2. Coupling scheme for the transitions to the excited states of ^{12}C and ^{15}N including their reorientations.

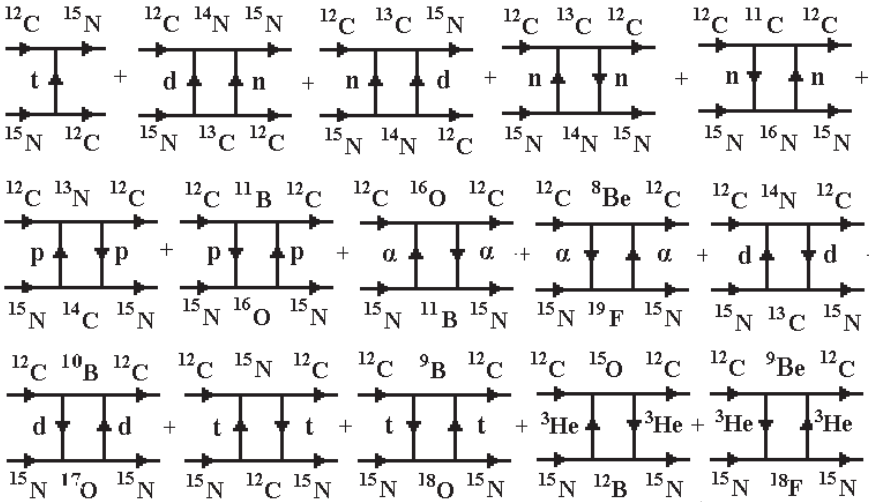


Fig. 3. Diagrams of one- and two-step transfers contributing to the $^{15}\text{N} + ^{12}\text{C}$ scattering calculations.

For the transfer reactions, the spectroscopic amplitudes S_x of transferred clusters or nucleons were obtained within the translational invariant shell model (TISM) [6] using code DESNA [7, 8]. The amplitudes S_x are listed in Table II (A is a nucleus composed of the core C and the transferred particle x).

TABLE I

Deformation parameters of ^{12}C and ^{15}N .

Nucleus	E_{ex} [MeV]	J^π	λ	δ_λ [fm]	$\beta_\lambda^{(a)}$	Ref.
^{12}C	4.439	2^+	2	-1.07	-0.37	[4]
^{15}N	5.270	$5/2^+$	3	1.0	0.32	[5]
	5.299	$1/2^+$	1	1.0	0.32	[5]
	6.324	$3/2^-$	2	1.0	0.32	[5]
	7.155	$5/2^+$	3	1.0	0.32	[5]
	7.301	$3/2^+$	1	1.0	0.32	[5]
	7.567	$7/2^+$	3	1.0	0.32	[5]
	8.313	$1/2^+$	1	1.0	0.32	this work
	8.571	$3/2^+$	1	1.0	0.32	this work

^(a) $\beta_\lambda = \delta_\lambda/R$ ($R = 1.25 A^{1/3}$ fm).

TABLE II

Spectroscopic amplitudes S_x of x -clusters in $A = C + x$ systems.

A	C	x	nL_j	S_x	A	C	x	nL_j	S_x
^{12}C	^8Be	α	$3S_0$	0.822	$^{15}\text{N}_{7.30}$	^{12}C	t	$1D_{3/2}$	0.641
^{12}C	^9Be	^3He	$2P_{3/2}$	1.224 ^(a)	$^{15}\text{N}_{7.56}$	^{12}C	t	$1G_{7/2}$	-0.393
^{12}C	^9B	t	$2P_{3/2}$	-1.224 ^(a)	$^{15}\text{N}_{7.56}$	^{12}C	t	$1G_{7/2}$	-0.393
^{12}C	^{10}B	d	$1D_3$	0.246	$^{15}\text{N}_{8.31}$	^{12}C	t	$2S_{1/2}$	0.641
^{12}C	^{11}B	p	$1P_{3/2}$	-1.706 ^(a)	$^{15}\text{N}_{8.57}$	^{12}C	t	$1D_{3/2}$	0.380
^{12}C	^{11}C	n	$1P_{3/2}$	1.706 ^(a)	^{15}N	^{13}C	d	$2S_1$	0.248 ^(a)
^{13}C	^{12}C	n	$1P_{1/2}$	0.601				$1D_1$	0.444 ^(a)
^{13}N	^{12}C	p	$1P_{1/2}$	0.601	^{15}N	^{14}C	p	$1P_{1/2}$	-0.598
^{14}N	^{12}C	d	$2S_1$	0.615	^{15}N	^{14}N	n	$1P_{1/2}$	-1.091 ^(a)
^{15}N	^{11}B	α	$2D_2$	0.435 ^(a)				$1P_{3/2}$	0.386
^{15}N	^{12}B	^3He	$1P_{1/2}$	0.254 ^(a)	^{15}O	^{12}C	^3He	$2P_{1/2}$	0.380
			$1P_{3/2}$	-0.090	^{16}N	^{15}N	n	$1D_{3/2}$	-0.270
^{15}N	^{12}C	t	$2P_{1/2}$	0.380	^{16}O	^{15}N	p	$1P_{1/2}$	-1.461 ^(a)
^{15}N	$^{12}\text{C}_{4.43}$	t	$2P_{3/2}$	-0.712 ^(a)	^{16}O	^{12}C	α	$3S_0$	0.544
			$1F_{5/2}$	0.466	^{17}O	^{15}N	d	$2P_2$	-0.552
$^{15}\text{N}_{5.27}$	^{12}C	t	$1D_{5/2}$	-0.393	^{18}O	^{15}N	t	$3P_{1/2}$	-0.261
$^{15}\text{N}_{5.29}$	^{12}C	t	$2S_{1/2}$	0.641	^{18}F	^{15}N	^3He	$3P_{1/2}$	-0.061
$^{15}\text{N}_{6.32}$	^{12}C	t	$2P_{3/2}$	0.380				$3P_{3/2}$	0.174 ^(a)
$^{15}\text{N}_{7.15}$	^{12}C	ts	$1D_{5/2}$	-0.393	^{19}F	^{15}N	α	$3S_0$	-0.638

^(a) $S_{\text{FRESCO}} = (-1)^{J_C + j - J_A} S_x = -S_x$.

The wave function of the bound state of cluster x was calculated by fitting the Woods–Saxon binding potential parameter V_0 to the cluster x binding energy in the $A = C + x$. The geometry parameters of the binding potentials were set to the following values: $a_V = 0.65$ fm, $r_V = 1.25 A^{1/3}/(C^{1/3} + x^{1/3})$ fm. The code FRESKO [9] was used for the CRC calculations.

The parameters of the real part of the optical model potential (1) were deduced from fitting it to the double-folding potential for the $^{15}\text{N}+^{12}\text{C}$ scattering system. This potential was calculated with the code DFOT [10], using charge distributions of the ^{15}N and ^{12}C nuclei adopted from Ref. [11].

The parameters of the optical model potential used in this work are compared to the similar potential for $^{14}\text{N}+^{12}\text{C}$ system obtained previously at 78 MeV [2] in Table III. While the real parts of the both potentials are quite similar at the strong absorption radius, the imaginary part for ^{15}N is much more absorptive at the surface. This suggests that inelastic processes are more important for ^{15}N than for ^{14}N .

TABLE III

Parameters of Woods–Saxon potentials.

$P + T$	E [MeV]	V_0 [MeV]	r_V [fm]	a_V [fm]	W_S [MeV]	r_W [fm]	a_W [fm]	Ref.
$^{15}\text{N}+^{12}\text{C}$	81	195	0.790	0.750	8.0	1.250	0.750	this work
$^{14}\text{N}+^{12}\text{C}$	78	100	0.920	0.770	38.5	1.290	0.260	[2]

The angular distribution of the measured $^{15}\text{N}+^{12}\text{C}$ elastic scattering at the energy $E_{\text{lab}}(^{15}\text{N}) = 81$ MeV and the results of the calculations for different nuclear processes are shown in Fig. 4. The curves show the results of the calculations for the $^{15}\text{N}+^{12}\text{C}$ potential scattering (curve ⟨pot⟩) and the results for the various transfer channels (see Fig. 3): transfer of t-cluster (curve ⟨t⟩), sequential transfers of protons and neutrons (curves ⟨nn⟩ and ⟨pp⟩, respectively), two-step d+n and n+d transfers (curve ⟨dn⟩) and α -cluster exchange (curve ⟨ $\alpha\alpha$ ⟩). The curves Σ_{WS} show the sum of all processes.

The potential scattering dominates the $^{15}\text{N}+^{12}\text{C}$ elastic scattering. The neutron- and t-cluster transfers contribute somewhat to the $^{15}\text{N}+^{12}\text{C}$ elastic scattering at the middle and back angles. The sum of all the processes (curve Σ_{WS}) describes the elastic scattering angular distribution slightly better than the pure optical model results.

The $^{15}\text{N}+^{12}\text{C}$ elastic scattering at the energy $E_{\text{lab}}(^{15}\text{N}) = 81$ MeV is compared with the $^{14}\text{N}+^{12}\text{C}$ elastic scattering at the energy $E_{\text{lab}}(^{14}\text{N}) = 78$ MeV [2] in the upper part of Fig. 5.

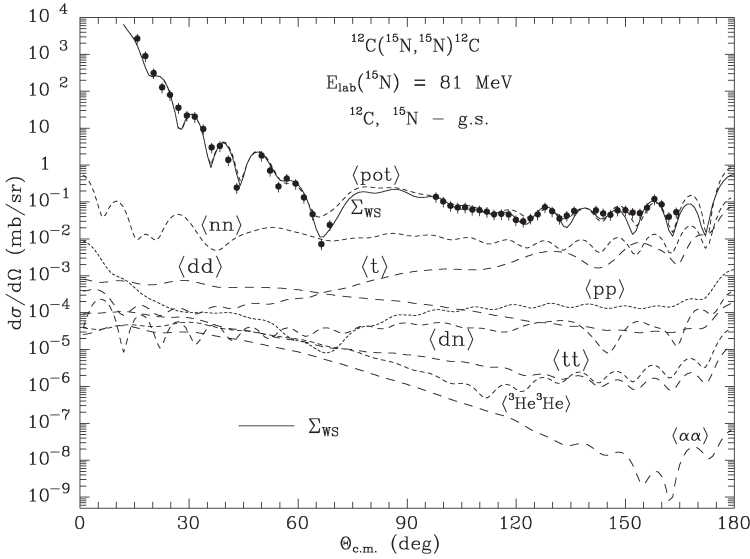


Fig. 4. Angular distributions of the $^{15}\text{N}+^{12}\text{C}$ elastic scattering. The dashed curves show the results of the calculations for different transfer channels. Curve Σ_{WS} shows the sum of all processes.

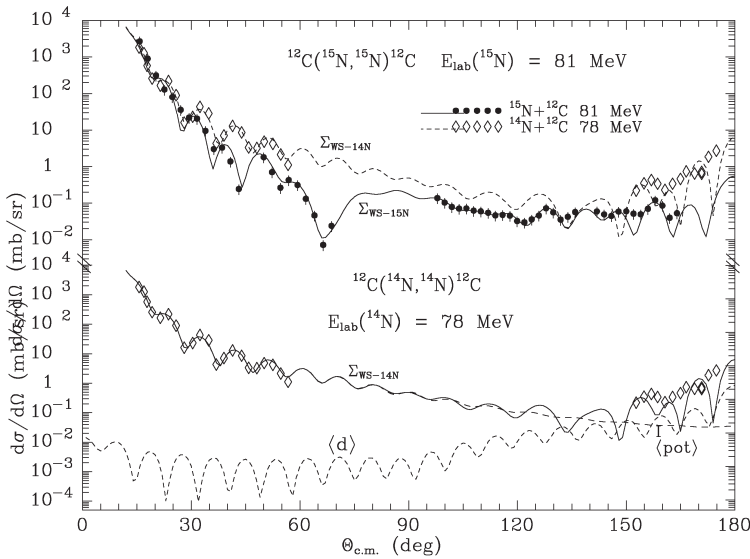


Fig. 5. Comparison of the $^{15}\text{N}+^{12}\text{C}$ elastic scattering at the energy $E_{\text{lab}}(^{15}\text{N}) = 81$ MeV (Fig. 4) with the $^{14}\text{N}+^{12}\text{C}$ elastic scattering at the energy $E_{\text{lab}}(^{14}\text{N}) = 78$ MeV [2].

The angular distributions of the $^{14}\text{N}+^{12}\text{C}$ elastic scattering data and corresponding CRC calculations with WS potential from [2] (Table III) are shown in the lower part of this figure. There, the dashed curve $\Sigma_{\text{WS-}^{14}\text{N}}$ shows the CRS calculations of a coherent sum for the $^{14}\text{N}+^{12}\text{C}$ potential scattering (curve ⟨pot⟩) and the d-cluster transfer (curve ⟨d⟩). One can see that the potential scattering dominates at angles $\theta_{\text{cm}} < 130^\circ$ and d-transfer contributes a lot to the $^{14}\text{N}+^{12}\text{C}$ elastic scattering at large angles. The contributions of two-step transfers to the $^{14}\text{N}+^{12}\text{C}$ elastic scattering are very small.

In the upper part of Fig. 5, one can see that the $^{15}\text{N}+^{12}\text{C}$ and $^{14}\text{N}+^{12}\text{C}$ angular distributions differ significantly at the angles ranging from 30 to 130 degrees as well as at the very backward angles. This difference must be attributed to the different structure of the nitrogen isotopes that causes differences in nucleus–nucleus interactions and nuclear process mechanisms.

The angular distributions of the $^{15}\text{N}+^{12}\text{C}$ inelastic scattering were measured for the 4.44 MeV (2^+) excited state of ^{12}C and for 5.27 MeV ($5/2^+$) + 5.30 MeV ($1/2^+$), 6.32 MeV ($3/2^-$), 7.16 MeV ($5/2^+$) + 7.30 MeV ($3/2^+$), 7.57 MeV ($7/2^+$) and 8.31 MeV ($1/2^+$) + 8.57 MeV ($3/2^+$) excited states of ^{15}N . These angular distributions are shown in Figs. 6 and 7. The curves show the results of CRC calculations using coupled-channel scheme presented in Fig. 2 as well as the t-transfer reaction $^{12}\text{C}(^{15}\text{N}, ^{12}\text{C})$. The form-factor $V_\lambda(r)$ (4) and deformation parameters δ_λ of ^{12}C and ^{15}N listed in Table I were

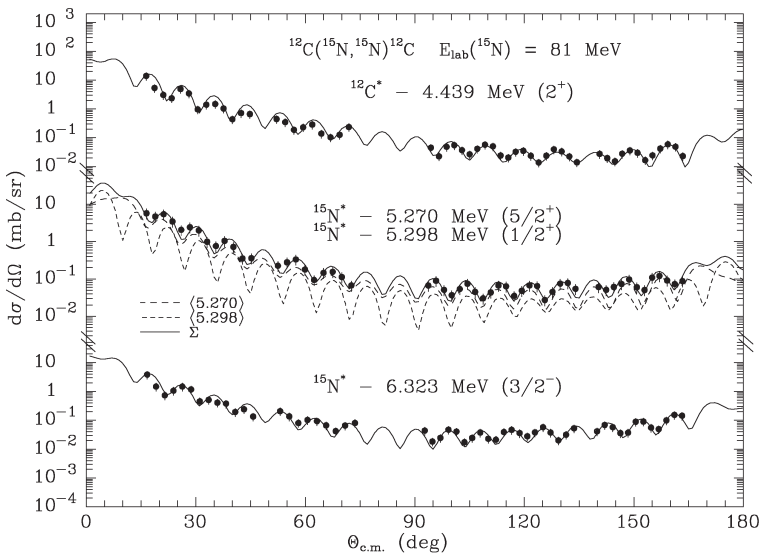


Fig. 6. Angular distributions of the $^{15}\text{N}+^{12}\text{C}$ inelastic scattering at the energy $E_{\text{lab}}(^{15}\text{N}) = 81$ MeV for the transitions to the excited states of ^{12}C and ^{15}N . The curves show the results of the calculations including the process of the t-transfer.

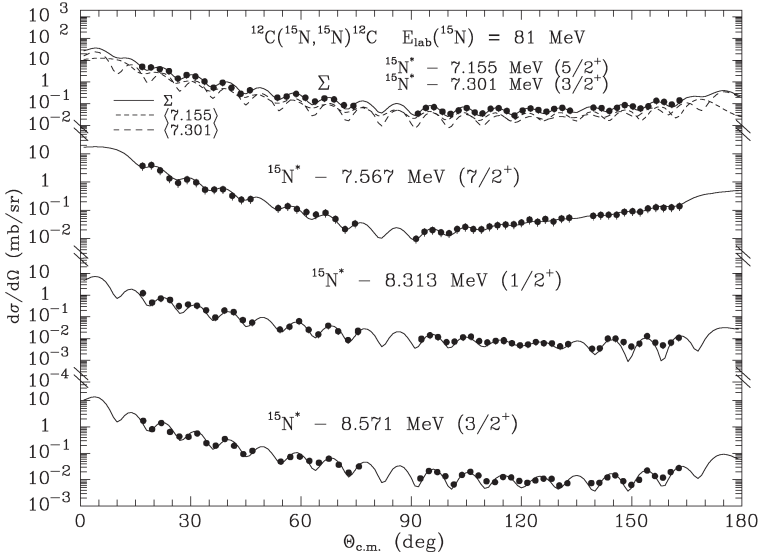


Fig. 7. The same as in Fig. 6 but for the other excited states of ^{15}N .

used. The t-cluster spectroscopic amplitudes for the system $^{15}\text{N} = ^{12}\text{C}+t$ in ground and excited states of ^{12}C and ^{15}N are listed in Table II. The incoherent sums of the CRC calculations for the unresolved in the experiment levels of ^{15}N are shown in Figs. 6 and 7 with the dashed curves. One can see that the calculations with the optical potential from Table III and using collective excitation model describe the $^{15}\text{N}+^{12}\text{C}$ inelastic scattering data rather well.

In order to study an energy dependence of the $^{15}\text{N}+^{12}\text{C}$ optical model potential parameters the previously reported $^{15}\text{N}+^{12}\text{C}$ elastic scattering data at the energies 22.4–31.4 MeV, measured at backward angles [1], were reanalyzed in this work using the model presented above. The deduced $^{15}\text{N}+^{12}\text{C}$ potential parameters are listed in Table IV and have only minor variations when compared to those obtained at 81 MeV. The results of the calculations are shown in Figs. 8 and 9. One can see that, again, the potential scattering (dashed curves) dominates at all energies. The solid curves show the elastic scattering together with the much smaller t-transfer contributions.

TABLE IV

Parameters of the $^{15}\text{N}+^{12}\text{C}$ potential.

E_{lab} [MeV]	V [MeV]	r_V [fm]	a_V [fm]	W_S [MeV]	r_W [fm]	a_W [fm]
22.4	193	0.87	0.80	4.4	1.29	0.80
22.6	193	0.87	0.80	4.4	1.29	0.80
23.4	198	0.85	0.80	5.5	1.27	0.80
24.0	198	0.85	0.80	5.5	1.27	0.80
24.8	198	0.85	0.80	5.5	1.27	0.80
25.2	200	0.85	0.80	5.5	1.25	0.80
26.8	200	0.85	0.80	5.5	1.25	0.80
28.6	200	0.85	0.80	6.0	1.25	0.80
29.4	200	0.84	0.80	6.0	1.25	0.80
31.4	200	0.80	0.80	5.5	1.20	0.80
81.0	195	0.79	0.75	8.0	1.25	0.75

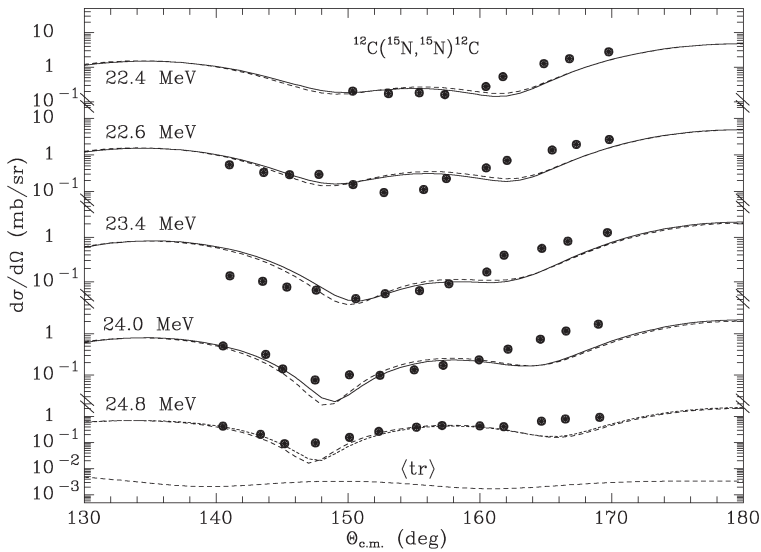


Fig. 8. Angular distributions of the $^{15}\text{N}+^{12}\text{C}$ elastic scattering at the energies $E_{\text{lab}}(^{15}\text{N}) = 22.4\text{--}24.8$ MeV [1]. The CRC calculations for potential scattering (dashed curves) and with inclusion of t-transfer (solid curves) are shown.

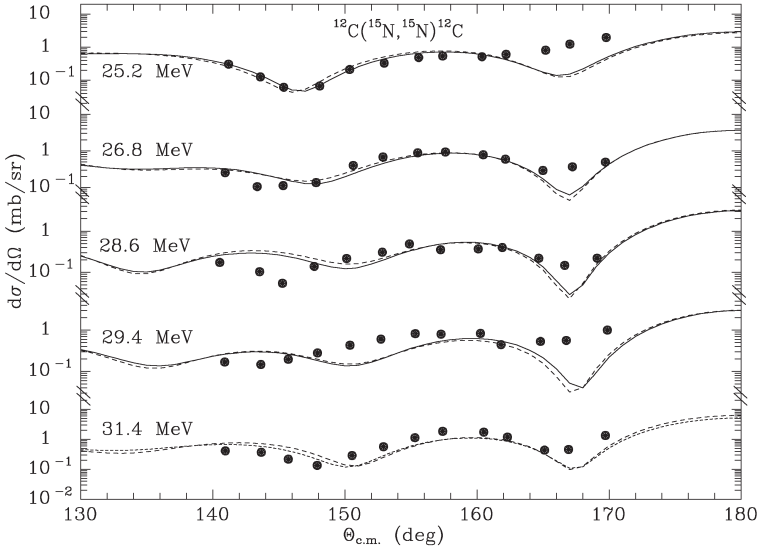


Fig. 9. The same as in Fig. 8 but for the energies $E_{\text{lab}}(^{15}\text{N}) = 25.2\text{--}31.4$ MeV [1].

4. Summary and conclusions

New experimental data for the $^{15}\text{N}+^{12}\text{C}$ elastic and inelastic scattering at the energy $E_{\text{lab}}(^{15}\text{N}) = 81$ MeV were measured for transitions to the ground and 4.396 MeV (2^+) excited states of ^{12}C as well as to the ground and 5.27 MeV–8.57 MeV excited states of ^{15}N .

The data were analyzed within the CRC method using WS potentials in the entrance and exit channels. Couplings to the inelastic channels and one- and two-step transfer reactions were included in the model calculations.

Optical Model potential of the WS shape was obtained for the $^{15}\text{N}+^{12}\text{C}$ scattering system and its energy dependence was studied. It was shown that the parameters of this potential vary very little with energy.

Quadrupole deformation parameters for the transitions to the 8.313 MeV and 8.571 MeV excited states of ^{15}N were extracted from the analysis. The other inelastic data were satisfactorily described using previously deduced deformation parameters.

Spectroscopic amplitudes for the various configurations in the light nuclei, ranging from ^{12}C to ^{19}F , were calculated by means of the translational invariant shell model. The effect of the transfer channels on the elastic and inelastic scattering differential cross sections was found to be small, even at very backward angles, with the triton transfer being the most important channel.

Comparison between the $^{14}\text{N}+^{12}\text{C}$ and $^{15}\text{N}+^{12}\text{C}$ elastic scattering data obtained at similar incident energies showed a significant difference that could be related to the different internal structure of the nitrogen isotopes.

REFERENCES

- [1] M.E. Ortiz *et al.*, *Phys. Rev. C* **22**, 1104 (1980).
- [2] W. Von Oertzen *et al.*, *Nucl. Phys. A* **143**, 34 (1970).
- [3] E. Piasecki *et al.*, Project ICARE at HIL, Annual report 2006, University of Warsaw, Heavy Ion Laboratory, Warszawa, 2007, p. 38.
- [4] J. Specht *et al.*, *Nucl. Phys. A* **171**, 65 (1971).
- [5] A.T. Rudchik *et al.*, *Nucl. Phys. A* **939**, 1 (2015).
- [6] Yu.F. Smirnov, Yu.M. Tchuvil'sky, *Phys. Rev. C* **15**, 84 (1977).
- [7] A.T. Rudchik, Yu.M. Tchuvil'sky, The code DESNA, Kiev Institute for Nuclear Researches report KIYAI-82-12, 1982.
- [8] A.T. Rudchik, Yu.M. Tchuvil'sky, *Ukr. Fiz. Zh.* **30**, 819 (1985).
- [9] I.J. Thompson, *Comput. Phys. Rep.* **7**, 167 (1988).
- [10] J. Cook, *Comput. Phys. Commun.* **25**, 125 (1982).
- [11] H. De Vries, C.W. De Jager, C. De Vries, *At. Data Nucl. Data Tables* **36**, 495 (1987).